

Two-photon polymerization as a potential manufacturing tool for biomimetic engineering of complex structures found in nature

Gordon Zyla¹,^{a,*} Alexander Kovalev²,^b Cemal Esen¹,^a
Andreas Ostendorf¹,^a and Stanislav Gorb²,^b

^aRuhr-Universität Bochum, Applied Laser Technologies, Bochum, Germany

^bChristian-Albrechts-Universität zu Kiel, Functional Morphology and Biomechanics, Kiel, Germany

Abstract. We report on the successful use of three-dimensional (3D) printing by two-photon polymerization to engineer optimized hierarchically composed surface structures at the micro- and nanoscale. The hierarchical composition of the printed structures was inspired by those found on the upper wing surface of blue-winged butterflies from the genus *Morpho*. In this way, the nanostructures and blue coloration of the organisms was mimicked, but less iridescence was achieved for biomimetic surfaces. Like the biological surface structures, the ones printed exhibited disorders characteristics. As a result, the blue colors generated by biomimetic structures displayed angle-insensitive optical properties similar to those of the *Morpho* wings. In addition, the great design freedom and simple workflow of the 3D printing technique enabled the fabrication of different structures at the microscale without modifying the dimension of the sub-structures at the nanoscale. Thus, it was possible to set the direction in which angle-insensitive coloration appeared to an observer. The morphology of biological and biomimetic surface structures was analyzed and compared using scanning electron microscopy. The optical properties of biological and engineered specimens were determined using angle-resolved spectroscopy. Furthermore, the coloration of biomimetic surfaces and the upper wing surface of *Morpho* butterfly was studied in different liquids. The results were compared, and potential application for biomimetic surfaces was discussed. © The Authors. Published by SPIE under a Creative Commons Attribution 4.0 International License. Distribution or reproduction of this work in whole or in part requires full attribution of the original publication, including its DOI. [DOI: [10.1117/1.JOM.2.3.031203](https://doi.org/10.1117/1.JOM.2.3.031203)]

Keywords: biomimetics; two-photon polymerization; 3D printing; structural colors; *Morpho* butterfly.

Paper 22009SS received Apr. 29, 2022; accepted for publication Aug. 12, 2022; published online Sep. 2, 2022.

1 Introduction

Two-photon polymerization (2PP) initiated by focused ultrashort pulsed laser radiation causes crosslinking of polymer chains inside transparent photosensitive resins due to nonlinear phenomena.^{1,2} As a result, an ellipsoidal volume of the exposed resin that is smaller than the focal volume of the laser beam is rendered insoluble to the solvent used to develop the material. Multiple ellipsoids, so-called voxels, can then be assembled by moving the resin relative to the focused laser beam or vice versa. In this way, 2PP enables the 3D printing of freeform structures with sub-micron features to explore novel applications in various fields, such as biophotonics,³ photonics,⁴ and optics.⁵ Another field for the use of 2PP is biomimetics. In this case, the excellent 2PP capabilities make it possible to mimic a broad diversity of functional surface structures inspired by nature. These structures often provide remarkable properties to organisms.^{6,7} Thus, they provide potential to engineer novel real-world applications.

Recently, 2PP has been used to realize bioinspired systems that foster properties, such as liquid transportation for drug delivery⁸ or wet and dry adhesion for space applications.^{9,10} In addition, 2PP has been proven to be suitable for generating so-called structural colors that result

*Address all correspondence to Gordon Zyla, zyla@lat.rub.de

from interference, diffraction, or scattering.^{11–16} In particular, the structural colors observed in organisms are highly interesting for, e.g., sensors, counterfeit protection, or displays applications¹⁷ because they often show extraordinary optical properties. For instance, these biological structural colors include the ultra-black color of the *Bitis gabonica*,^{18,19} the iridescent green coloration of the butterfly *Chrysina gloriosa*,²⁰ and the angle-insensitive blue coloration of the butterflies from the genus *Morpho*,^{21–23} to name a few. Most organisms, including those mentioned, use hierarchically organized structures at the micro- and nanoscale to generate structural colors.²⁴ However, the remarkable optical properties are often additionally caused by disorder characteristics in the surface structures.^{22,25,26}

Due to the disorder characteristics, the morphology of such biological photonic surfaces are highly complex.^{22,24,27} Accordingly, their mimicry requires an approach with high spatial resolution and high flexibility to make the resulting colors available for the technical purposes mentioned above. Although structural color can be produced due to self-assembled colloidal particles, the particles' size and shape limit the overall structural geometry to be produced.²⁸ Therefore, lithography^{29–33} and deposition techniques^{34,35} have been considered as the best option, most recently. However, these techniques require multiple workflows, vacuum atmosphere, exposure masks, harsh chemicals, or a cleanroom, thus delimiting them in their flexibility. In contrast, those cumbersome tools do not have to be applied for 2PP, making the approach and the process handling more suitable and easy in this case.

This paper describes how 2PP was used to generate blue coloration with similar optical properties to those of the blue *Morpho* butterflies, though the 2PP resolution is considered to be too low for this purpose. Although our previous works dealt with similar topics,^{13–15} this paper further strengthens the high potential of using 2PP for biomimetic research. Unlike our previous works, the optical properties of *Morpho didius* (*M. didius*) were studied in detail for various viewing directions and viewing angles. The findings were then used to print two structures with different geometries at the microscale but identical substructures at the nanoscale. The use of the two different structures enabled to set the *Morpho*-like optical properties for a specific viewing direction or uniformly in all directions. Thus, the paper demonstrates the high flexibility of the 2PP process to print complex structures with less effort than the lithography or deposition approaches mentioned above. The morphology of biological and 2PP structures was analyzed using scanning electron microscopy (SEM). The optical properties of the blue wing structure of the *M. didius* and engineered structures were measured using angle-resolved spectroscopy. Moreover, the coloration of 2PP structures and the butterfly's wing structure was studied in different liquid environments.

2 Morphology and Optical Properties of the Blue Wing Surface of the Butterfly *Morpho didius*

The blue butterflies from the genus *Morpho* are among the most famous specimens in the field of structural colors because of their intense blue coloration on their upper wing structure that appears almost angle-insensitive.^{21,22} Using the *M. didius* as an example, the unique optical properties arise from the wing scales [see Fig. 1(a)], classified into cover and ground scales. While the base material of the cover scales is transparent, the ground scales' base material appears brownish due to melanin pigmentation.^{21,22} In addition, both types of wing scales are equipped with hierarchically composed surfaces structures at the micro- and nanoscale, so-called ridges and lamellas [see SEM images in Fig. 1(a)], forming multilayer systems using air and chitin-protein composite of the cuticle. The thickness of the single air ($n = 1$) and chitin-protein composite ($n = 1.56$) layer is ~ 150 and 50 nm, respectively.²¹ Therefore, the blue coloration of *M. didius* primarily arises from multilayer interference. In this case, it is worth mentioning that the ground scales mainly produce the blue color of the specimen because they possess a higher number of ridges than the cover scales.²²

Furthermore, the surface structures exhibit disorder characteristics that further determine the butterfly's optical properties by diffraction and scattering. For example, ridges are often tilted, which, in turn, may cause the ridges to differ in their heights up to 200 nm. In addition, the tilt of the ridges also affects the lamellas to be not entirely periodically arranged [see Fig. 1(a), SEM images] that is why the air gaps between the lamellas vary in their size.²² As a result, unlike

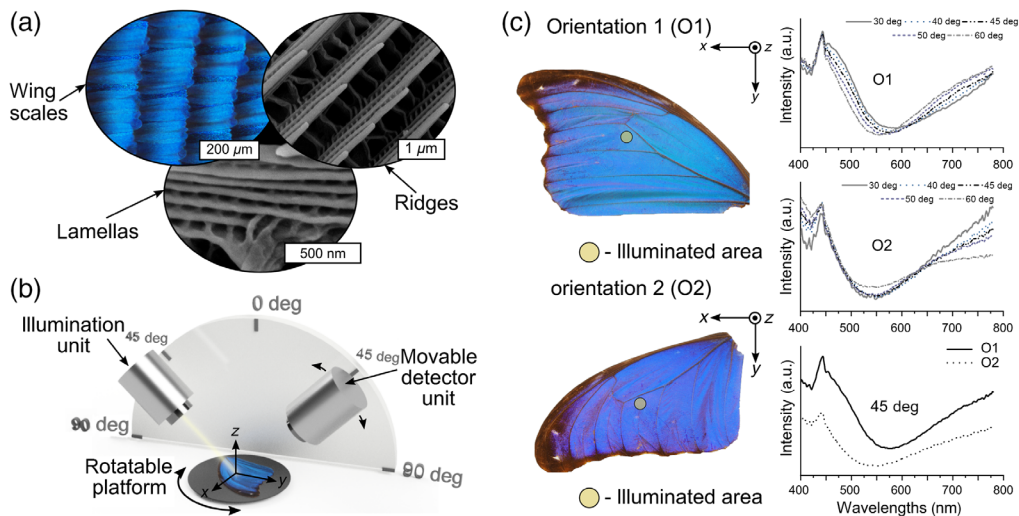


Fig. 1 Morphology of *M. didius*' surface structures and the optical properties of its blue wing surface. (a) The blue structural coloration of *M. didius* results from hierarchically composed structures found on the wing scales on its upper wing structure. The hierarchically composed structures, so-called ridges and lamellas, form multilayer systems with disorder characteristics. (b) Experimental setup for the spectrometer used to study the optical properties of biological and engineered samples for different viewing directions and viewing angles. The samples were illuminated at 45 deg using white light. The illumination area had a diameter of 1 mm. (c) Coloration and optical properties of the *M. didius*' left upper wing structure for different viewing angles (30 deg to 60 deg) and viewing directions. For this purpose, the wing structure of the *M. didius* was orientated differently (O1, O2) in the setup shown in (b).

highly ordered multilayer systems, visible light of almost the same color is reflected in a wide angular range as if each ridge scatters the light independently.^{21,22}

The extraordinary optical properties of *M. didius* (left upper wing structure, female, collected at Tingo Maria, 700 m, Peru, 03/2004) are presented by the photographs and the spectra shown in Fig. 1(c). The photographs were taken by a camera (Olympus, OMD 10 mark iii). Spectra were recorded using a homebuilt setup [see Fig. 1(b)]. This setup enabled determining the optical properties of all samples presented in this work as a function of an observer's viewing angle and viewing direction. For angle-resolved analysis, the position of the detector unit was varied in an angular range between 30 deg and 60 deg, referring to the device's surface normal. For studying the optical properties as a function of the viewing direction, the samples were differently orientated using a rotatable platform. In this case, the detector unit was fixed at 45 deg, as shown in Fig. 1(b). For all experiments, the samples were illuminated from the opposite at 45 deg using white light. A detailed overview of the setup's design, components, and postprocessing methods for spectral analysis is given by the reference.¹³

As shown in Fig. 1(c), the orientation of wing structure was varied in the setup shown in Fig. 1(b) (O1, O2) to determine the *M. didius*' optical properties as described already. The area marked in yellow in Fig. 1(c) represents the white-light illumination (diameter = 1 mm). The area illuminated at the butterfly's wing structure was the same for O1 and O2. The upper graphs show the reflection characteristics as a function of an observer's viewing angle. Here, the peak at 450 nm, which arises from multilayer interference, appears almost angle-insensitive in a range of 30 deg for each orientation. However, it becomes obvious that the spectral characteristics between O1 and O2 spectra slightly differ. For example, O1 spectra show less intensity for shorter wavelengths between 400 and 450 nm compared to O2 spectra and higher wavelengths between 700 and 800 nm, referring to the peak intensity at 450 nm. In addition, the spectral width of the reflection maximum at the blue wavelength range is larger in the O1 spectrum than in the O2 spectrum. As a result, the upper wing structure of the *M. didius* shows bluish iridescent characteristics, as also proven by literature^{21,22,24,36} and the photographs in Fig. 1(c).

The iridescent properties can be attributed to the following criteria. First, in the case of the *M. didius*, the ground scales have slightly different optical properties when the cover scales do

not cover them completely,²² although they do not lose their angle-insensitive optical properties in this case. Second, though the orientation of wing scales follows a pattern, as illustrated in the microscope image in Fig. 1(a), it can vary in all three dimensions depending on the region studied and the surface characteristics of the wing structure. Moreover, the ridges are also specifically orientated on the wing scales [see SEM image in Fig. 1(a)] and possess an inclination between 7 deg and 10 deg relative to the plane of the scales.²¹ Thus, in brief, the spectral characteristics and the intensity of the reflection can differ in specific viewing direction [see lower graph in Fig. 1(c)] because they are determined by the number and orientation of *M. didius*' wing scales contributing to the color formation process. However, the blue color appears almost angle-insensitively when observed for various viewing angles in a specific viewing direction.

3 Mimicry of the *Morpho didius*' Surface Structures Using Two-Photon Polymerization

From the findings achieved in Sec. 1, it can be derived that an angle-insensitive blue coloration would appear less bluish iridescent if one can control the orientation and number of the ridges on a less rough surface than the butterfly's wing structure. Thus, it would also be possible to set the angle-insensitive optical properties of the blue color for either only specific viewing directions or uniformly for all directions. 3D printing by 2PP provides the implementation of such possibilities, as presented in the following, only by printing *Morpho*-inspired structures arranged to different geometries at the microscale.

Although the resolution of the standard 2PP technique is too low to fabricate replicas of the *M. didius* ridges, the interference-assisted 2PP (INT-2PP) method has proven to be suitable.^{16,37,38} This method enables the realization of sub-100 nm features in the cross-section of polymerization volumes if the printing process is performed, e.g., in a thin film of a photosensitive resin [see Fig. 2(a)]. The axial modulation of a printed structure occurs at specific positions z according to the equation $z = k\lambda_0/(4n)$ ^{16,37} due to the interference of the incident laser radiation and the partly reflected laser radiation on the lower surface of the thin film, where k is a positive integer, λ_0 the central wavelength of the laser, and n is the refractive index of the photoresist. However, the thickness of the polymer layers within the modulated structure depends on the laser power used and determines the dimension of air gaps simultaneously. In this way, INT-2PP thus enables the printing of similar multilayer systems as those found on the wing surface of *M. didius* [see Fig. 2(b)].

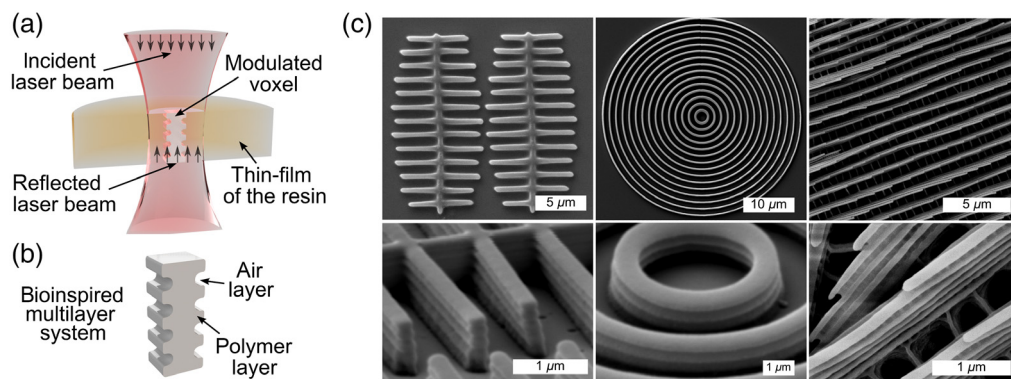


Fig. 2 Mimicry of the *M. didius* lamellar ridges using interference-assisted 2PP. (a) In a thin film of a transparent photosensitive resin the incident and the partly reflected beam on the lower boundary surface of the film interfere. Thus, the voxel created by 2PP is modulated in its cross-section. (b) Modulated voxels generate multilayer systems mimicking the photonic structures of the *M. didius*. (c) Engineered structures printed by INT-2PP, so-called arcs and rings, are illustrated in the left and central SEM images, respectively. The right SEM images show the lamellar ridges of the *M. didius* for a better comparison. Primary microstructures are shown in the upper SEM images. The lower SEM images present the nanostructures in the cross-section of the microstructures.

In this work, FemtoBond 4B ($n = 1.51$) was used as the resin for generating thin films on a coverslip with a thickness of $\sim 1 \mu\text{m}$ using spin coating. More details about the generation of such thin films can be found in reference.¹⁵ The film thickness was measured using white-light interferometry (TMS 1200, Polytec). For resin processing by INT-2PP, ultrashort pulsed laser radiation (100 fs, rep. rate = 82 MHz, a wavelength of 780 nm, Tsunami, Spectra-Physics) was tightly focused by an oil-immersed microscope objective ($100\times$ /NA 1.4, Plan-Apo, Nikon). The bioinspired structures were fabricated by scanning the laser beam in the photoresist with the use of a 2D galvo scanner (hurrysca II 14, Scanlab). In addition, a mechanical stage (ANT 130-XY, Aerotech) was used for stitching that enabled the fabrication of an arbitrary number of bioinspired structures on one coverslip, as presented later. After the 2PP process, the samples were developed in isopropanol for 10 min to remove the unexposed material. More detailed information on the 2PP setup is described in the reference.¹³ For all experiments, INT-2PP was performed using an average power of 10 mW and a galvo scanner speed of 1.4 mm s^{-1} .

The different geometries of bioinspired structures fabricated by INT-2PP can be seen on the upper left and central SEM images in Fig. 2(c). The lower SEM images present the associated nanostructures in the cross-section of the primary microstructures. On the right-hand side, SEM images show the ridges and lamellas of the scales in the *M. didius*. These images were added for a better comparison between biological and bioinspired structures. The SEM images of the 2PP structures were taken using Zeiss EVO MA 15. Beforehand, the 2PP samples had been covered with 10-nm thick Au-Pd using sputter-coating (SC7620, Quorum Technologies). In order to image the biological structures shown in Figs. 1(a) and 2(c), the SEM Hitachi S-4800 was used.

The 2PP structures that show more lines only for one direction were named arcs [see Fig. 2(c), left]. The others were called rings [see Fig. 2(c), center]. When one compares these structures with biological ones [see Fig. 2(c), right], the *Morpho* structures and 2PP structures were similar hierarchically composed. In the bioinspired multilayer system, single polymer layers and air gaps were ~ 80 and 100 nm thick, respectively, as previously investigated,¹⁵ thus reflecting the light in the blue region of the visible spectrum, as presented later. In addition, it is worth mentioning that 2PP structures were fabricated with an average laser power close to the polymerization threshold, thus, fostering the existence of imperfections in typically perfectly printed 2PP structures due to the low degree of polymerization³⁹ or the fluctuation of the average power of an ultrashort pulse laser.^{40–43} Therefore, the thickness of single polymer layers varied,^{13–15} and some bioinspired structures were tilted [see Fig. 2(c), bottom left]. In other words, due to these effects, the bioinspired structures showed similar disorder characteristics as those mentioned for the scales of the *M. didius* (see Sec. 2). The resulting coloration of 2PP structures and their optical properties are presented in Fig. 3. The color images of the processed samples shown in Fig. 3(a) were captured using a light microscope (Eclipse LV 100, Nikon) in combination with a $5\times$ objective (LU Plan Fluor, Nikon) as described in reference.¹³ The spectra were recorded using the setup shown in Fig. 1(b) and described in Sec. 2.

The processed areas shown in Fig. 3(a) were composed of multiple arcs or rings stitched periodically. The structure type and orientation used for the specific areas can be depicted from the insets in Fig. 3(a). Each area had a size of $250 \times 250 \mu\text{m}^2$ and was produced in 3 h. As mentioned before, the structures generated intense blue coloration as the wings of the *M. didius* due to the presence of multilayers. In addition, their optical properties matched the organism's one because the disorders of biomimetic and biological surfaces structures were similar. Thus, both colored areas printed by 2PP displayed almost angle-insensitive optical properties over an angular range of $\sim 30^\circ$ with a peak at 450 nm [see Fig. 3(b)]. However, the 2PP structures reflect the light more broadband than the wing structure of *M. didius* [see Fig. 1(c)] because, unlike the 2PP structures, the organisms' ground scales exhibit melanin pigmentation that absorb the transmitted light.³⁶ In contrast, the optical properties of 2PP structures did not show any reflection at high visible wavelengths because the 2PP structures were fabricated on less rough substrates. In the case of the *M. didius*, the reflection at higher visible wavelengths shown in Fig. 1(c) might result from interference or diffraction at strongly distorted surface structures.

As discussed at the beginning of this section, the two bioinspired structures printed by INT-2PP enabled to set angle-insensitive optical properties for specific viewing directions. For example, the arcs exhibited more lines in one than in the other direction [see Fig. 2(c)]. Thus, depending on the orientation of the arcs inside the processed area, i.e., as presented for O1 or O2 in

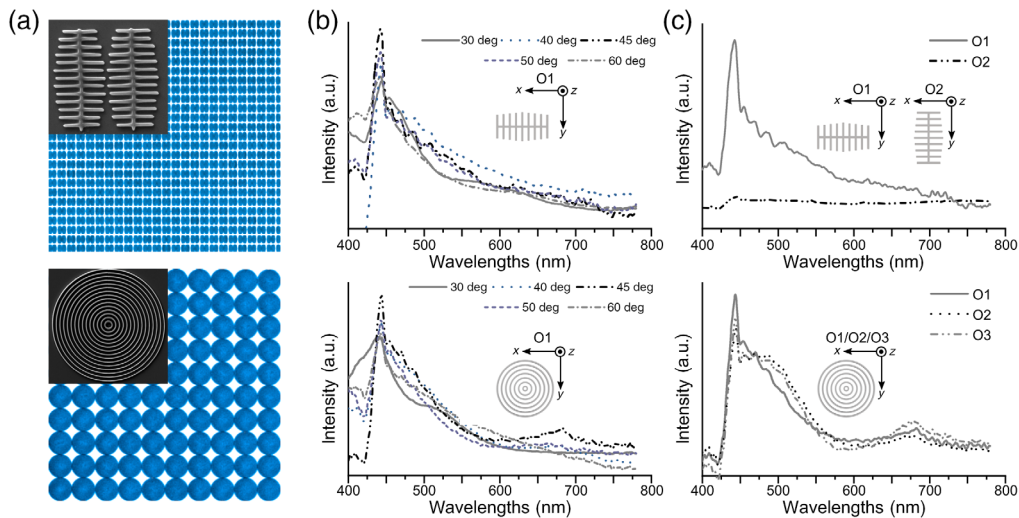


Fig. 3 Blue structural color generated by bioinspired 2PP structures and their optical properties. (a) Resulting color generated by bioinspired 2PP structures (arcs and rings). Each color area has a size of $250 \times 250 \mu\text{m}^2$. The color images were captured using a light microscope (Eclipse LV 100, Nikon) in combination with a $5\times$ objective (LU Plan Fluor, Nikon). The SEM images shown in the insets illustrate which structure type was used to process the associated blue area. (b) Optical properties of the processed areas shown in (a) for different viewing angles. (c) Optical properties of the processed areas shown in (a) for different viewing directions. All spectra were measurement using the setup shown in Fig. 1(b). The detector unit was fixed at 45 deg, and the samples were illuminated from the opposite at 45 deg using white light. The position of the blue areas for different orientation (O1–O3) are referred to the coordinate system shown in Fig. 1(b).

Fig. 3(c), a different amount of lines would contribute to the color formation process when the processed area would be tilted around a specific axis.^{14,15} Thus, only if the arcs were orientated as shown for O1, an intense reflection in the blue wavelengths spectra could be measured using the setup shown in Fig. 1(b). In contrast to the arcs, the rings are highly symmetric. Therefore, as shown in the bottom image of Fig. 3(c), all spectra measured were almost similar for different orientations (O1–O3) that had been chosen randomly. Thus, the blue coloration could be observed from every direction almost uniformly because the same amount of artificial lamellas would always contribute to the color formation if the sample is tilted at a specific angle. The differences between the spectra resulted from structural defects due to the sample handling in this case. The same applies to differences between the arc and ring spectra shown in Fig. 3(b) when comparing the angle-insensitive optical properties for a specific detection angle.

4 Coloration of Biological and Biomimetic Surfaces in Liquid Environments

As described in Sec. 2, the intense blue coloration of the *Morpho* butterflies originates from lamellar ridges on the wing scales generating a multilayer system of air ($n = 1$) and chitin-protein composite ($n = 1.56$).²¹ Thus, if one looks perpendicularly at the ridges of *Morpho*, the visible light will be reflected according to the equation $\lambda = 2(n_1d_1 + n_2d_2)$,⁴⁴ resulting in the constructive interference of light at a wavelength of $\sim\lambda = 450 \text{ nm}$. In this case, n and d define the refractive index and single layer's thickness of the corresponding material, respectively. To prove that the color indeed results only from the lamellar ridges, a change of the *Morpho* wing coloration was successfully studied by replacing air with different liquids, e.g., ethanol.²² According to the equation mentioned, a different coloration resulted from a change of the interference conditions due to the higher refractive index of the liquid compared to air. In this work, a similar experiment was conducted, as shown in Fig. 4(a), to analyze and compare the resulting coloration from bioinspired structures and *M. didius* ridges in isopropanol. Thus, it was possible to estimate the applicability of bioinspired structures for fluid sensors or

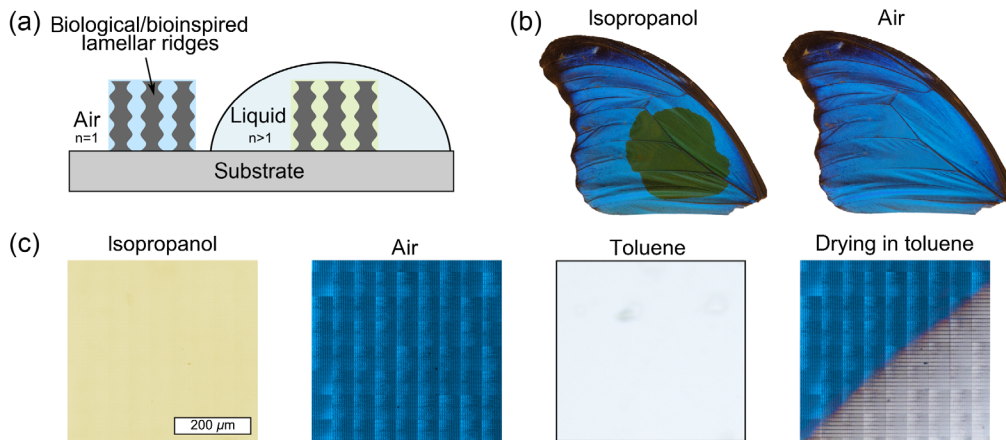


Fig. 4 Resulting structural colors of biological and bioinspired structures in different liquid environments. (a) Schematic illustration of the procedure used to analyze the upper wing coloration of *M. didius* and engineered areas processed by INT-2PP. (b) Upper wing coloration of *M. didius* in isopropanol ($n = 1.379$) and air ($n = 1$). The photographs were taken by a camera (Olympus, OMD 10 mark iii). (c) Coloration of bioinspired structures in isopropanol ($n = 1.379$), air ($n = 1$), toluene ($n = 1.497$), and during drying in toluene. Every experiment, i.e., every color analysis in different liquids, was performed using the same sample. The size of the area processed by INT-2PP was $500 \times 500 \mu\text{m}^2$. The color images were captured using a light microscope as described in Sec. 3 and in the caption of Fig. 3.

counterfeit protection. For this purpose, an area of $500 \times 500 \mu\text{m}^2$ was processed in 15 h using the same parameters mentioned in Sec. 3. In this context, arcs were used, but ones more densely stitched than before to generate a completely closed color area. Afterward, the biological specimen shown in Fig. 1 and 2PP structures were covered by isopropanol ($n = 1.379$, Sigma Aldrich). The volume of isopropanol used to cover the *M. didius* wing scales was $100 \mu\text{l}$ set by a pipette. For studying the resulting coloration from 2PP structures, less isopropanol ($20 \mu\text{l}$) was used because the size of the areas processed by 2PP was smaller than the butterfly's wing structure. For color monitoring, the same camera as mentioned in Sec. 2 was used for taking photographs of the butterfly's wing structure. For recording the images of the 2PP samples, the light microscope mentioned in Sec. 3 was used, but this time with a $2.5\times$ objective (L Plan, Nikon).

As illustrated in the left photograph in Fig. 4(b), the droplet of isopropanol intentionally caused a change of the *M. didius* wing coloration from blue to dark green with a peak at $\lambda = 560 \text{ nm}$ calculated by the equation mentioned above. In addition, the coloration change is reversible, as presented in the right image of Fig. 4(b). Thus, blue color returned back when the wing structure was thoroughly dried.

In contrast, a yellowish color was achieved when isopropanol was put on the area processed by 2PP, which was blue in air [see Fig. 3(c)]. However, the yellowish color did not match the multilayer interference equation mentioned. In this context, the low degree of polymerization of bioinspired structures was identified as a major reason. Therefore, the liquid caused the single lines of the bioinspired structures to swell.^{45,46} In this way, the interference condition in the bioinspired interference system was differently modified by the liquid than in the biological one, thus reflecting the light in the yellow spectral range.

Furthermore, to provide clear evidence that colors generated by INT-2PP only result from the bioinspired structures, the color of the processed area was further studied using $20 \mu\text{l}$ of toluene ($n = 1.497$, Sigma Aldrich). As clearly demonstrated by the third microscope image in Fig. 4(c), the intense blue color disappeared when the toluene covered the bioinspired structures. Thus, the sample became transparent since toluene and the 2PP material ($n = 1.51$) have a similar refractive index. However, the intense blue color reappeared when the toluene began to evaporate, as illustrated by the right image in Fig. 4(c). It is worth mentioning that this image illustrates the sample after the fifth repetition of the experiment, and the intense blue color remained observable. Therefore, analyzing the effect of different liquids on 2PP photonic structures is

robust and reproducible. In addition, upon closer inspection of the microscope images associated with the toluene experiments, a light bluish color was identified in the image shown the sample immersed in toluene. We assume the scattering of light on impurities and defects within the bioinspired structures caused this low intense coloration because the refractive index of toluene and the 2PP material did not entirely match. Moreover, we suppose this effect was not achieved when the sample began to dry for different reasons. First, the original bioinspired photonic system reflected the light more intensely. Therefore, the intense blue color might have suppressed the light bluish color of transparent areas when capturing the right microscope image shown in Fig. 4(c). Second, describing the entire color formation during the drying of such 2PP structures is highly complex. For instance, some 2PP structures were thoroughly dried and reflected the light in the intense blue color, whereas other structures slowly started to shrink due to the evaporation of the liquid or were still entirely or partly covered by toluene of different volumes. Thus, the color of the processed area shown in the right microscope image in Fig. 4(c) was determined by multiple physical effects, such as scattering, thin-film interference, and multilayer interference. In addition, each physical effect was determined by various interference and scattering conditions for the reasons mentioned during the complex drying process, which surpassed the light blue color.

5 Discussion and Conclusion

In this work, laser-based additive manufacturing by 2PP was used to print 3D structures mimicking the lamellar ridges found on the wing scales of the blue butterflies from the genus *Morpho*. For this purpose, 2PP was combined with the interference-assisted method to modify the cross-section of processed polymer volume at the nanoscale. Thus, the bioinspired structures were hierarchically composed like the *Morpho* ridges and built a multilayer system that reflected the light in an intense blue coloration [see Fig. 3(c)]. In addition, the structures printed by INT-2PP also exhibited the same disorder characteristics as the butterfly [see Fig. 2(c)]. The disorder characteristics in the bioinspired structures were attributed to the low average laser power used for printing. Thus, the 2PP structures had a low polymerization degree affecting many structures to tilt on the coverslip during the development process [see Fig. 2(c)]. As a result, blue structural colors generated by bioinspired 2PP structures displayed angle-insensitive optical properties similar to those observed for the blue *Morpho* butterflies, using the *M. didius* in this work as an example [compare Figs. 1(c) and 3(b)].

Unlike in our previous works,^{13–15} in this study, the optical properties of the scales of the *M. didius* were analyzed in detail using a homebuilt spectrometer setup [see Fig. 1(b)]. More precisely, the butterflies' optical properties were studied as a function of the viewing angle and viewing direction. Therefore, as also proven by literature,^{21,22,36} it could be demonstrated that indeed the blue coloration of the *M. didius*' wings is angle-insensitive for a specific viewing direction [see Fig. 1(c), upper graphs]. However, the color displayed iridescence, if the viewing direction was varied [see Fig. 1(c), lower graph]. The iridescent properties were attributed to many complex factors (see Sec. 2), influenced mainly by the natural surfaces roughness of the butterfly's wing structure. Those findings obtained from the study of structures in the real were then used to avoid the iridescent properties resulting from bioinspired structures that exactly mimic the biological blueprint. Thus, 2PP further enabled to produce structures, which demonstrates angle-insensitive blue coloration for specific viewing angles or uniformly for all directions [see Fig. 3(c)]. For this purpose, two structures, referred to as arcs and rings, were used. These structures consisted of a specific number of artificial *Morpho*-like ridges arranged to different geometries at the microscale. However, they exhibited identical nanostructures in their cross-section because they were fabricated using the same 2PP process parameters [see Fig. 2(c)].

Furthermore, the resulting coloration generated by bioinspired structures was analyzed in different liquid environments. In contrast to the wing structure of a *M. didius* that changed its color from blue to green in isopropanol [see Fig. 4(b)], an area printed by INT-2PP surprisingly changed its color from blue to yellow in the same liquid [see Fig. 4(c)], although green was expected. The formation of the yellow color can be traced back to the swelling of the 2PP structures with a low polymerization degree in liquids.^{45,46} Therefore, bioinspired interference systems were differently modified than biological ones. Due to the swelling of the material,

bioinspired photonic systems show limitations to be applied for various sensor applications. However, the change of coloration or its disappearance using liquids [see Fig. 4(c)] could be an excellent and straightforward method to verify the colors' originality. In particular, this robust and reproducible test as described in Sec. 4 would be highly crucial when such colors are used in counterfeit protection, one of the most promising applications as presented by Zyla et al.¹⁴ In addition, this work further underlines the high potential for the use of such colors for counterfeit protection since the high flexibility of 2PP enables the generation of blue structural colors with angle-insensitive optical properties for specific viewing directions or uniformly in all directions. As a result, numerous opportunities arise to generate highly complex patterns in a simple workflow. In this context, it is important to mention that not only blue but also green coloration with angle-insensitive optical properties can be fabricated by only modifying the 2PP parameters used to process FemtoBond 4B ($n = 1.51$).¹⁵

Furthermore, the generation of bioinspired structures that reflect the light in yellow and red and have the same optical properties as the blue-winged butterflies from the genus *Morpho* is also theoretically conceivable using INT-2PP, for instance, by using laser radiation with a central wavelength $\lambda_0 > 780$ nm. Then, the axial modulation of a printed structure that follows the equation $z = k\lambda_0/(4n)$ ^{16,37} could be modified differently, thus increasing the air gaps' dimensions inside the bioinspired photonic system. In contrast, the polymer layer thickness and the polymerization degree of the structures can be kept the same. For this purpose, a Ti:Sa oscillator⁴⁷ or novel ultrashort lasers operating at $\lambda_0 = 830$ nm⁴⁸ are potentially suitable. Another promising procedure to generate yellow and red *Morpho*-like coloration is the use of novel high refractive index hybrid materials and, if applicable, to process them using modern tunable fs lasers.⁴⁹ For instance, Nanoscribe has recently developed the photoresist IP-n162 ($n = 1.62$), which can be used to fabricate microoptics.⁵⁰ In addition, a refractive index modification of a hybrid material is also feasible by calcination using pyrolysis as a post-processing.^{51,52} For example, the refractive index of SZ2080™ (IESL-FORTH, Greece), a typically used 2PP hybrid material, can be tuned up to a value of 1.617 in this way.^{52,53} In this context, it is worth mentioning that the calcination of SZ2080™ simultaneously affects an isotropic shrinkage of 2PP-printed nanostructures by up to 70%.⁵⁴ Thus, this post-processing provides a high scope to continue modifying the bioinspired structures shown in this work.

In conclusion, the results presented here further strengthen that 2PP is highly suitable as a manufacturing tool for biomimetic research. Due to its high flexibility by generating arbitrary structures with high resolution and recent improvements in photoresists as aforementioned, which is still an ongoing process, 2PP enables unprecedented possibilities nowadays and in the future to study the broad diversity of functional surface structures found in nature. Although standard 2PP setups still suffer from high throughput, recent optimization of the 2PP process, e.g., by spatiotemporal focusing using a digital mirror device,⁵⁵ can significantly speed up the printing. Thus, the use of 2PP is also conceivable for the fabrication of real-world biomimetic products soon.

Acknowledgment

The authors declare that there is no conflict of interests regarding the publication of this manuscript.

References

1. M. Farsari and B. N. Chichkov, "Two-photon fabrication," *Nat. Photonics* **3**, 450–452 (2009).
2. K. Sugioka, "Hybrid femtosecond laser three-dimensional micro- and nanoprocessing: a review," *Int. J. Extrem. Manuf.* **1**, 012003 (2019).
3. C. Maibohm et al., "Multi-beam two-photon polymerization for fast large area 3d periodic structure fabrication for bioapplications," *Sci. Rep.* **10**, 8740 (2020).
4. O. Tsilipakos et al., "Split-cube-resonator-based metamaterials for polarization-selective asymmetric perfect absorption," *Sci. Rep.* **10**, 17653 (2020).

5. T. Gissibl et al., “Two-photon direct laser writing of ultracompact multi-lens objectives,” *Nat. Photonics* **10**, 554–560 (2016).
6. B. Bhushan, “Biomimetics: lessons from nature—an overview,” *Phil. Trans. R. Soc. Lond. Ser. A: Math. Phys. Eng. Sci.* **367**(1893), 1445–1486 (2009).
7. P. Vukusic and J. R. Sambles, “Photonic structures in biology,” *Nature* **424**, 852–855 (2003).
8. C. Plamadeala et al., “Bio-inspired microneedle design for efficient drug/vaccine coating,” *Biomed. Microdevices* **22**, 8 (2020).
9. Y. Wang et al., “Strong wet and dry adhesion by cupped microstructures,” *ACS Appl. Mater. Inter.* **11**(29), 26483–26490 (2019).
10. J. F. Busche et al., “Controllable dry adhesion based on two-photon polymerization and replication molding for space debris removal,” *Micro Nano Eng.* **7**, 100052 (2020).
11. B.-K. Hsiung et al., “Rainbow peacock spiders inspire miniature super-iridescent optics,” *Nat. Commun.* **8**(1), 2278 (2017).
12. B.-K. Hsiung et al., “Tarantula-inspired noniridescent photonics with long-range order,” *Adv. Opt. Mater.* **5**(2), 1600599 (2017).
13. G. Zyla et al., “Generation of bioinspired structural colors via two-photon polymerization,” *Sci. Rep.* **7**(1), 17622 (2017).
14. G. Zyla et al., “Biomimetic structural coloration with tunable degree of angle-independence generated by two-photon polymerization,” *Opt. Mater. Express* **9**(6), 2630 (2019).
15. G. Zyla et al., “Structural colors with angle-insensitive optical properties generated by *Morpho*-inspired 2PP structures,” *Appl. Phys. A* **126**, 740 (2020).
16. H. Gu et al., “Wide-gamut biomimetic structural colors from interference-assisted two-photon polymerization,” *ACS Appl. Mater. Interfaces* **13**(50), 60648–60659 (2021).
17. F. Chen et al., “Bio-inspired structural colors and their applications,” *Chem. Commun.* **57**, 13448–13464 (2021).
18. M. Spinner et al., “Snake velvet black: hierarchical micro- and nanostructure enhances dark colouration in *Bitis rhinoceros*,” *Sci. Rep.* **3**, 1846 (2013).
19. M. Spinner et al., “Non-contaminating camouflage: multifunctional skin microornamentation in the West African Gaboon viper (*Bitis rhinoceros*),” *PLoS One* **9**(3), e91087 (2014).
20. V. Sharma et al., “Structural origin of circularly polarized iridescence in jeweled beetles,” *Science* **325**(5939), 449–451 (2009).
21. P. Vukusic et al., “Quantified interference and diffraction in single *Morpho* butterfly scales,” *Proc. R. Soc. Lond. B-Biol. Sci.* **266**(1427), 1403–1411 (1999).
22. S. Kinoshita, S. Yoshioka, and J. Miyazaki, “Physics of structural colors,” *Rep. Prog. Phys.* **71**(7), 076401 (2008).
23. H. Ghiradella, “Light and color on the wing: structural colors in butterflies and moths,” *Appl. Opt.* **30**(24), 3492–3500 (1991).
24. S. L. Burg and A. J. Parnell, “Self-assembling structural colour in nature,” *J. Phys. Condens. Matter* **30**(41), 413001 (2018).
25. V. E. Johansen et al., “Photonics in nature: from order to disorder,” in *Functional Surfaces in Biology III. Biologically-Inspired Systems*, S. Gorb and E. Gorb, eds., Vol. 10, Springer, Cham (2017).
26. M. Rothhammer et al., “Tailored disorder in photonics: learning from nature,” *Adv. Opt. Mater.* **9**(19), 2100787 (2021).
27. J. Sun, B. Bhushan, and J. Tong, “Structural coloration in nature,” *RSC Adv.* **3**(35), 14862 (2013).
28. P. Liu et al., “Self-assembled colloidal arrays for structural color,” *Nanoscale Adv.* **1**(5), 1672–1685 (2019).
29. R. H. Siddique et al., “Theoretical and experimental analysis of the structural pattern responsible for the iridescence of *Morpho* butterflies,” *Opt. Express* **21**(12), 14351–14361 (2013).
30. R. H. Siddique et al., “Fabrication of hierarchical photonic nanostructures inspired by *Morpho* butterflies utilizing laser interference lithography,” *Opt. Mater. Express* **5**(5), 996 (2015).

31. R. A. Potyrailo et al., "Towards outperforming conventional sensor arrays with fabricated individual photonic vapour sensors inspired by *Morpho* butterflies," *Nat. Commun.* **6**, 7959 (2015).
32. S. Zhang and Y. Chen, "Nanofabrication and coloration study of artificial *Morpho* butterfly wings with aligned lamellae layers," *Sci. Rep.* **5**, 16637 (2015).
33. P. Huo et al., "Photorealistic full-color nanopainting enabled by a low-loss metasurface," *Optica* **7**(9), 1171–1172 (2020).
34. K. Chung et al., "Flexible, angle-independent, structural color reflectors inspired by *Morpho* butterfly wings," *Adv. Mater.* **24**(18), 2375–2379 (2012).
35. B. Song et al., "Reproducing the hierarchy of disorder for *Morpho*-inspired, broad-angle color reflection," *Sci. Rep.* **7**, 46023 (2017).
36. H. Ghiradella, "Hairs, bristles and scales," in *Microscopic Anatomy of Invertebrates*, F. W. Harrison and M. Locke, eds., Vol. 11: Insecta, pp. 257–287, Wiley, New York (1998).
37. Q.-Q. Liu et al., "Tunable multilayer submicrostructures fabricated by interference assisted two-photon polymerization," *Appl. Phys. Lett.* **111**(22), 223102 (2017).
38. B. Mills et al., "Single-pulse multiphoton fabrication of high aspect ratio structures with sub-micron features using vortex beams," *Appl. Phys. A* **108**(3), 651–655 (2012).
39. Y. Liu et al., "Deformation behavior of foam laser targets fabricated by two-photon polymerization," *Nanomaterials-Basel* **8**(7), 498 (2018).
40. J. Fischer and M. Wegener, "Three-dimensional optical laser lithography beyond the diffraction limit," *Laser Photonics Rev.* **7**(1), 22–44 (2013).
41. K. Takada, H.-B. Sun, and S. Kawata, "Improved spatial resolution and surface roughness in photopolymerization-based laser nanowriting," *Appl. Phys. Lett.* **86**(7), 071122 (2005).
42. X. Zhou, Y. Hou, and J. Lin, "A review on the processing accuracy of two-photon polymerization," *AIP Adv.* **5**(3), 030701 (2015).
43. J. Serbin et al., "Femtosecond laser-induced two-photon polymerization of inorganic-organic hybrid materials for applications in photonics," *Opt. Lett.* **28**(5), 301–303 (2003).
44. S. Kinoshita and S. Yoshioka, "Structural colors in nature: the role of regularity and irregularity in the structure," *ChemPhysChem* **6**(8), 1442–1459 (2005).
45. K. Takada et al., "Size-dependent behaviors of femtosecond laser-prototyped polymer micronanowires," *Opt. Lett.* **34**(5), 566–568 (2009).
46. S. Rekšytė et al., "Microactuation and sensing using reversible deformations of laser-written polymeric structures," *Nanotechnology* **28**(12), 124001 (2017).
47. J. Klein and J. Kafka, "The flexible research tool," *Nat. Photonics* **4**, 289 (2010).
48. G. Zyla et al., "Two-photon polymerization with diode lasers emitting ultrashort pulses with high repetition rate," *Opt. Lett.* **45**, 4827–4830 (2020).
49. M. Tromayer et al., "Wavelength-optimized two-photon polymerization using initiators based on multipolar aminostyryl-1,3,5-triazines," *Sci. Rep.* **8**, 17273 (2018).
50. M. Schmid et al., "3D printed hybrid refractive/diffractive achromat and apochromat for the visible wavelength range," *Opt. Lett.* **46**, 2485–2488 (2021).
51. A. Vyatskikh et al., "Additive manufacturing of high-refractive-index, nanoarchitected titanium dioxide for 3D dielectric photonic crystals," *Nano Lett.* **20**(5), 3513–3520 (2020).
52. D. Gonzalez-Hernandez et al., "Laser 3D printing of inorganic free-form micro-optics," *Photonics* **8**(12), 577 (2021).
53. M. Nogami, "Glass preparation of the ZrO₂-SiO₂ system by the sol-gel process from metal alkoxides," *J. Non-Crystall. Solids* **69**, 415–423 (1985).
54. G. Seniutinas et al., "Beyond 100 nm resolution in 3D laser lithography—post processing solutions," *Microelectron. Eng.* **191**, 25–31 (2018).
55. P. Sommers et al., "Rapid, continuous projection multi-photon 3D printing enabled by spatiotemporal focusing of femtosecond pulses," *Light Sci. Appl.* **10**, 199 (2021).

Gordon Zyla is currently a postdoctoral fellow in the Farsari Lab at IESL-FORTH, Crete, Greece. He studied mechanical engineering at Ruhr University Bochum (RUB), Germany. He recently received his PhD in mechanical engineering from RUB in 2020. In his PhD, his research focused on the 3D printing of biologically inspired surface structures to generate structural colors. In 2021, he was awarded the Gateway Fellowship from the RUB Research School.

Alexander Kovalev obtained his PhD in 2005 from the Institute of the Theoretical and Experimental Biophysics, Russian Academy of Science. He has been a postdoc in the Functional Morphology and Biomechanics group at University of Kiel, Germany, since 2009. Currently, he is an engineer in that group. Previously, he was a postdoc student in the 3rd Institute of Physics at the University of Stuttgart, Germany.

Cemal Esen studied mechanical engineering at University of Duisburg, Germany. He received his PhD in mechanical engineering at RUB in 1997, where he studied the production and characterization of polymer microparticles. In 2008, he finished his habilitation at RUB. Currently, he is a professor in Applied Laser Technologies at RUB. His research focuses on novel laser techniques for measurement and material processing applications.

Andreas Ostendorf is currently a full professor in Applied Laser Technologies at RUB, Germany. He studied electrical engineering at Leibniz University Hannover, Germany. In 2000, he received his PhD in mechanical engineering from Leibniz University. Also, in 2000, he was appointed as executive director at Laser Zentrum Hannover, Germany. In 2003, he was elected a member of the German Scientific Laser Society. From 2004–2019, he was also a member of the board of directors at Laser Institute of America (LIA). He is a fellow of LIA and SPIE.

Stanislav Gorb is currently a professor and director at the Zoological Institute of Kiel University, Germany. He received his PhD in zoology and entomology at the Ukrainian Academy of Sciences in Kiev, Ukraine. Afterward, he worked as a researcher in Germany, e.g., as a group leader at the Max Planck Institute for Developmental Biology in Tübingen, among other things. His research focuses on morphology, structure, biomechanics, physiology, and evolution of surface-related functional systems in organisms, as well as the development of biologically inspired technological surfaces and systems.